Purely excitonic lasing in ZnO microcrystals: Temperature-induced transition between exciton-exciton and exciton-electron scattering

doi: 10.1103/PhysRevB.96.125306

Purely excitonic lasing in ZnO microcrystals: Temperature-induced transition between exciton-exciton and exciton-electron scattering

Ryosuke Matsuzaki,[1] Haruka Soma,[1] Kanae Fukuoka,[1] Kanako Kodama,[1] Akifumi Asahara,[2] Tohru Suemoto,[2] Yutaka Adachi,[3] and Takashi Uchino[1,*]

[1]*Department of Chemistry, Graduate School of Science, Kobe University, 1-1 Rokkodai, Nada, Kobe 657–7501, Japan*

[2]*Institute for Solid State Physics, University of Tokyo, 5-1-5 Kashiwanoha, Kashiwa, Chiba 277–8581, Japan*

[3]*Optoelectronic Materials Group, Optical and Electronic Materials Unit, National Institute for Materials Science, 1–1 Namiki, Tsukuba, Ibaraki 305–0044, Japan*

(Received 25 March 2017; revised manuscript received 2 September 2017; published 27 September 2017)

Since the seminal observation of room-temperature laser emission from ZnO thin films and nanowires, numerous attempts have been carried out for detailed understanding of the lasing mechanism in ZnO. In spite of the extensive efforts performed over the last decades, the origin of optical gain at room temperature is still a matter of considerable discussion. In this work, we show that a ZnO film consisting of well-packed micrometer-sized ZnO crystals exhibits purely excitonic lasing at room temperature without showing any symptoms of electron-hole plasma emission, even under optical excitation more than 25 times above the excitonic lasing threshold. The lasing mechanism is shifted from the exciton-exciton scattering to the exciton-electron scattering with increasing temperature from 3 to 150 K. The exciton-electron scattering process continues to exist with further increasing temperature from 150 to 300 K. Thus, we present distinct experimental evidence that the room-temperature excitonic lasing is achieved not by exciton-exciton scattering, as has been generally believed, but by exciton-electron scattering. We also argue that the long carrier diffusion length and the low optical loss nature of the micrometer-sized ZnO crystals, as compared to those of ZnO nanostructures, plays a key role in showing room-temperature excitonic lasing.

DOI: 10.1103/PhysRevB.96.125306

I. INTRODUCTION

Among other lasing materials, ZnO is one of the most well-studied optical semiconductors because of its relatively large exciton binding energy E_b of about 60 meV [1,2]. Previously, there have been a number of studies on room-temperature laser emission from ZnO nanostructures, such as thin films [3–7], nanowires [8–11], nanodisks [12–14], and nanoparticles [15–18]. Two main mechanisms are generally invoked as responsible for optical gain: excitonic and electron-hole plasma (EHP) processes [1,2]. An EHP state is formed when the density of electron-hole pairs exceeds the Mott density n_M, where screening reduces the Coulomb interaction sufficiently that no bound excitonic states are present. Accordingly, room-temperature EHP emission is observed commonly in most ZnO nanostructures under sufficiently high optical excitation [3–7,11,17,18]. On the other hand, room-temperature excitonic lasing is achieved almost exclusively in high-quality samples, such as ZnO epitaxial layers [3–7] and highly faceted ZnO nanorods [19,20]. Note also that the exciton-dominated regime generally overlaps with the EHP-dominated regime; that is, the EHP emission begins to appear as the excitation density exceeds nearly twice of the excitation threshold for excitonic lasing [3–7,19,20]. This is most likely because, even in such high-quality ZnO nanomaterials, rather high excitation density close to n_M is required for excitonic laser action to compensate heavy optical loss inherent to these nanostructures. Thus, realization of pure excitonic lasing at room temperature would be difficult for ZnO nanostructured materials, as has been proven in the case of ZnO nanowires [11]. To make matters more challenging, the origin of the excitonic gain in ZnO at room temperature is still controversial [9,21]. The room-temperature excitonic lasing was originally attributed to the exciton-exciton (ex-ex) scattering process [3–7]. However, Klingshirn *et al.* [22,23] later argued that the ex-ex process, which is the dominant excitonic lasing process at low temperatures ($T <\sim 100$ K), will not survive up to room temperature; they [22,23] proposed that the ex-ex process will be transferred to another one, such as those based on exciton-LO phonon (ex-LO) or exciton-electron (ex-el) scattering, with increasing temperature, although the direct experimental evidence of the transition has not been presented yet.

In order to shed new light on the excitonic lasing process in ZnO, temperature-dependent and time-resolved photoluminescence (PL) measurements were carried out for the micrometer-thick ZnO film grown on a *c*-plane (0001) sapphire substrate. In addition, emission properties of a bulk ZnO single crystal with a dimension of $10 \times 10 \times 0.5$ mm and an 85-nm-thick ZnO thin film grown on an *a*-plane ($11\bar{2}0$) sapphire substrate were also investigated for comparison. Although little attention has been paid to lasing characteristics of the ZnO microcrystals previously [24–26], these microcrystals have notable advantages over the often-studied nanostructured materials to identify the origin of the excitonic optical gain. We demonstrate that individual ZnO microcrystals in the film can serve as effective resonators to show laser action owing to the fact that their size is larger than the emission wavelength [27]. The observed feedback mechanism is incoherent and is hence different from the one reported for ZnO nanocrystals, where random laser with coherent feedback is possible due to multiple interparticle scattering [27]. It should be noted,

*uchino@kobe-u.ac.jp

however, that the lasing line due to incoherent feedback represents the maximum of the net gain of the medium [27,28] and is particularly useful to explore the origin of the gain mechanism. From a detailed analysis of the temperature-dependent lasing spectra of the micrometer-thick ZnO film, we present convincing experimental evidence that the excitonic lasing in ZnO at room temperature is not induced by the ex-ex scattering but by the ex-el scattering. We also demonstrate that as the temperature increases from 3 to 150 K, lasing scheme is changed continuously from the ex-ex to the ex-el process, which then continues to exist at temperatures up to room temperature.

II. EXPERIMENTAL PROCEDURES

A. Sample preparation

A micrometer-thick ZnO film was prepared by thermo-chemical reduction of ZnO in the presence of reducing elements such as Li and B. Synthesis was carried out in a box-type electric furnace. In a typical reaction process, ∼1 g of high-purity ZnO powders (99.999%) and an equal molar amount of Li (or B) were put in a cylindrical alumina crucible. A *c*-plane sapphire substrate was located above the crucible as a lid. The furnace was then evacuated to a pressure down to ∼30 Pa and purged with high-purity argon gas (99.999%). The temperature of the furnace was raised to 1000 °C at a rate of ∼15 °C/min and kept constant at 1000 °C for 1 h under flowing argon environment. After the heating process, a ZnO film with a thickness of ∼3 μm was deposited on the sapphire substrate. From quantitative analysis conducted by x-ray photoelectron spectroscopy (XPS), we confirmed that the ZnO films contain no traces of reducing agents (Li and B), indicating that these films are nominally undoped ZnO.

An 85-nm-thick film was grown on an *a*-plane sapphire substrate by pulsed laser deposition (PLD) using the fourth harmonic ($\lambda = 266$ nm) of a Nd-doped yttrium aluminum garnet (Nd:YAG) laser with a pulse width of 5 ns, a repetition rate of 5 Hz, and an averaged fluence of about 1 J/cm^2. The growth rate of the film was ∼0.02 nm/pulse. *a*-plane sapphire is frequently chosen as a substrate to grow high-quality *c*-axis-oriented ZnO thin films because the fourfold of the ZnO "*a*"-lattice constant fits perfectly to the "*c*"-lattice constant of sapphire with a mismatch of less than 0.08% at room temperature [29]. The target for the PLD system was made in-house from ZnO powder. The pressure in the growth chamber was kept at 2 mPa by introduction of pure oxygen gas. The substrate temperature was kept at 700 °C.

B. Characterization

Powder x-ray diffraction (XRD) patterns were obtained with a diffractometer (Rigaku, SmartLab) using Cu Kα radiation. Scanning electron microscopy (SEM) was conducted with a scanning electron microscope (JEOL, JSM-5510). XPS measurements were performed with an XPS Microprobe (ULVAC-PHI PHI X-tool).

PL measurements were carried out with a gated image intensified charge-coupled device (Princeton Instruments, PI-MAX:1024RB) and 1800 or 300 lines/mm grating by using the third harmonic (355 nm) of a Q-switched YAG laser (Spectra Physics, INDI 40, pulse width ∼10 ns, repetition rate 10 Hz) as an excitation source. During the PL measurements, the laser pulse was irradiated onto the sample surface without focusing the beam (beam spot size of ∼7 mm), and the emission signal from the front surface was monitored. The sample temperature was controlled in an optical cryostat system in the temperature range from 3 to 300 K.

We also performed time-resolved PL measurements at room temperature with a femtosecond Ti:sapphire laser system with an optical parametric amplifier (OPA). We used the 350-nm pulses generated with OPA (Light Conversion, TOPAS-C), which was seeded by a 1-kHz Ti:sapphire regenerative amplifier system (Spectra Physics, TSUNAMI 3160C and Spitfire) producing 120-fs pulses at 800 nm. This femtosecond laser system, combined with a streak camera (Hamamatsu Photonics, C5680), was used to obtain time-resolved photoluminescence (TRPL) spectra. The overall time resolution of the measuring system was ∼4 ps. For the TRPL measurements, the samples were excited by a femtosecond laser pulse focused to a spot size of ∼200-μm diameter. Time-integrated PL signals were also measured with the same optical arrangement as the TRPL, except that a fiber-optic spectrometer was used to monitor the emitted signals.

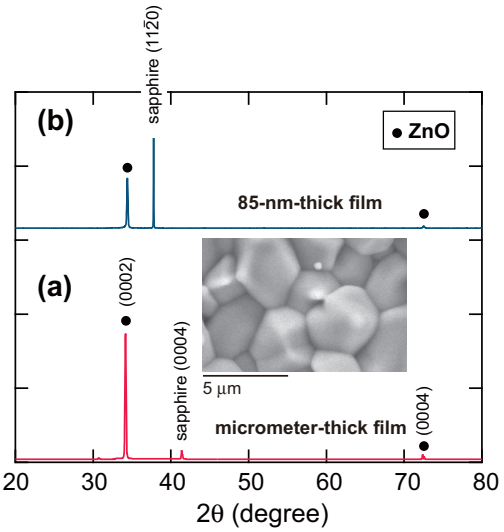

FIG. 1. XRD patterns of (a) the micrometer-thick ZnO film and (b) the 85-nm-thick ZnO film. The inset show a typical SEM image of the micrometer-thick ZnO film.

III. RESULTS

A. Structural characteristics

XRD patterns of the micrometer-thick and the 85-nm-thick film samples are given in Fig. 1. Aside from the peak from sapphire substrate, both the samples exhibit only (000*l*) ZnO peaks ($l = 2$ and 4) in the respective XRD patterns, demonstrating that these film samples are highly *c*-axis oriented. The inset of Fig. 1 presents a typical SEM image of the micrometer-thick film. The film consists of closely packed micrometer-sized grains with smooth hexagonal facets on the surface. Thus, the present micrometer-thick sample can be regarded as a collection of well-grown ZnO crystals both in

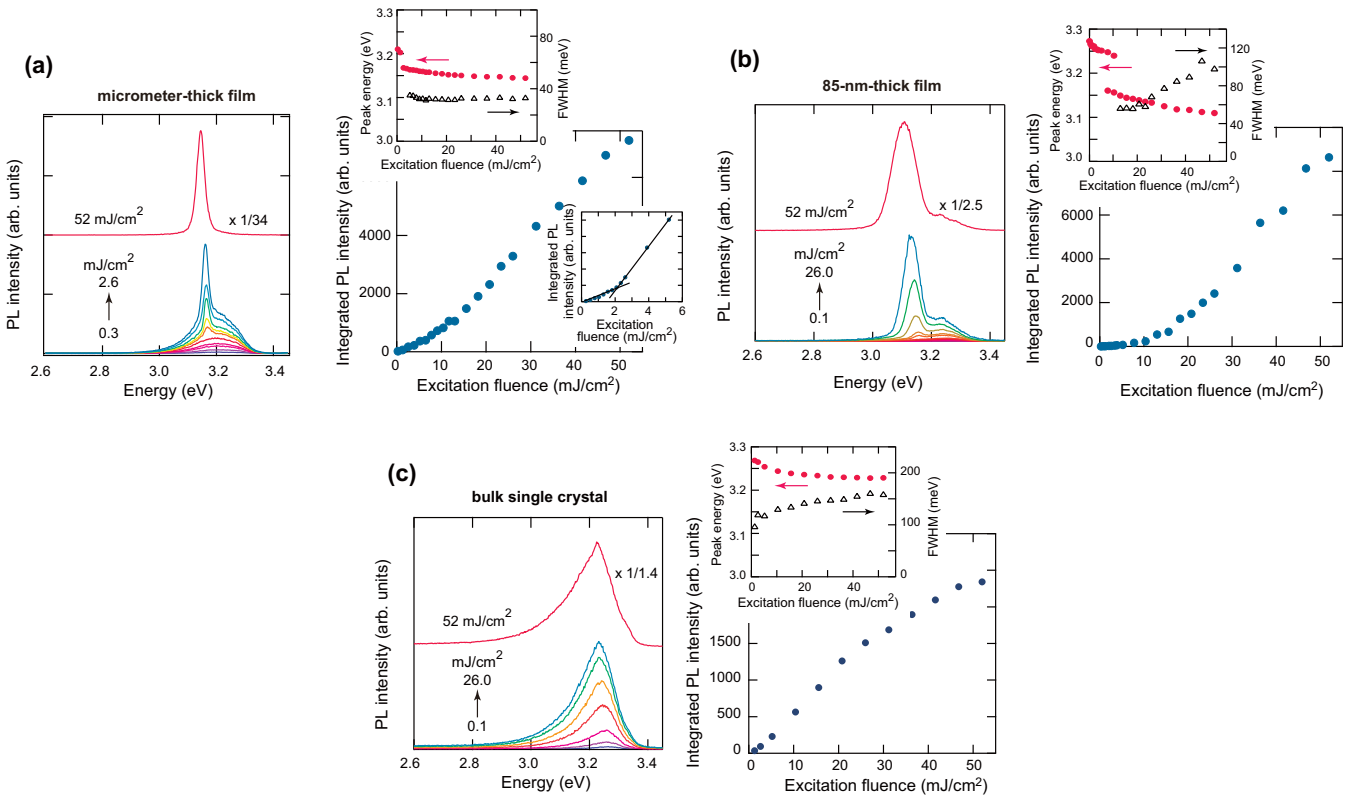

FIG. 2. Excitation fluence dependence of the room-temperature PL characteristics of (a) the micrometer-thick ZnO film, (b) the 85-nm-thick ZnO film, and (c) the bulk ZnO single crystal. The third harmonic ($\lambda = 355$ nm) of a 10-ns pulsed Nd:YAG laser was used as an excitation source. Left and right panels show a series of PL spectra obtained under different excitation fluences and the corresponding spectrally integrated PL intensity, respectively. The upper insets in the right panels indicate the excitation fluence dependence of the FWHM (right axis) and the peak position (left axis) of the PL band. As for the FWHM for the film samples, the value for the narrow component is shown. The lower inset in the right panel of (a) is a magnified plot near the threshold region.

the lateral and longitudinal direction in the micrometer length scale.

B. PL characteristics at room temperature

Room-temperature PL spectra of the micrometer-thick film, the 85-nm-thick film, and the bulk single crystal for increasing excitation fluence I_{exc} are shown in Fig. 2. All the results shown in Fig. 2 were obtained using the third harmonic (355 nm) of a nanosecond pulsed Nd:YAG laser (pulse width ~10 ns, repetition rate 10 Hz) as an excitation source. As shown in Fig. 2(a), the integrated intensity of the near-band-edge emission for the micrometer-thick film sample exhibits a laserlike behavior with a threshold I_{exc}^{th} of excitation fluence of $\sim 2\,mJ/cm^2$ [refer also to the lower inset in the right panel of Fig. 2(a)], accompanied by peak narrowing from about 120-meV full width at half maximum (FWHM) below I_{exc}^{th} to about 30-meV FWHM above I_{exc}^{th} [see the upper inset in the right panel of Fig. 2(a)]. Considering that the size of the ZnO crystallites ($\sim 3\,\mu m$) is much larger than the emission wavelength, the observed laserlike behavior will result from the random laser emission with incoherent (intensity) feedback within the respective particles [27,28]. On the other hand, spectral narrowing with excitation intensity was not observed either in the 85-nm-thick ZnO film [Fig. 2(b)] or in the bulk ZnO single crystal [Fig. 2(c)]. Note, however, that the 85-nm-thick film sample displays a nonlinear increase in intensity accompanied by spectral broadening and redshift with increasing I_{exc}, as often observed for EHP lasing in ZnO nanostructured materials [1–7]. Thus, the results shown in Fig. 2 demonstrate that the expected lasing characteristics of ZnO depend strongly on the size and morphology of the crystals.

To further confirm the occurrence of laser action in the micrometer-thick film sample, we carried out time-resolved PL measurements using ~120-fs pluses at 350 nm from a Ti:sapphire laser with an optical parametric amplifier (see Fig. 3). Similar to the case of ns-pulse excitation, excitation with fs-laser pulses induces a laserlike behavior in terms of both the PL spectral feature and decay characteristics. When the excitation fluence is relatively low ($I_{exc} <\sim 0.5\,mJ/cm^2$), only a broad PL band with a FWHM of ~140 meV and a decay time constant of 125 ps is observed in the energy region around 3.3 eV (see the red decay line in the inset of Fig. 3). For sufficiently high excitation fluences ($I_{exc} >\sim 4\,mJ/cm^2$), a sharp PL component with a FWHM of ~30 meV and a decay time constant of <4 ps (our instrumental resolution) is developed on the lower-energy side of the broad emission band (see the blue decay line in the inset in Fig. 3). This short decay time of <4 ps is comparable to the decay time observed previously for the excitonic emission in ZnO nanorods at room temperature [19,20]. It is hence reasonable to conclude that that the sharp peak observed from the micrometer-thick ZnO film

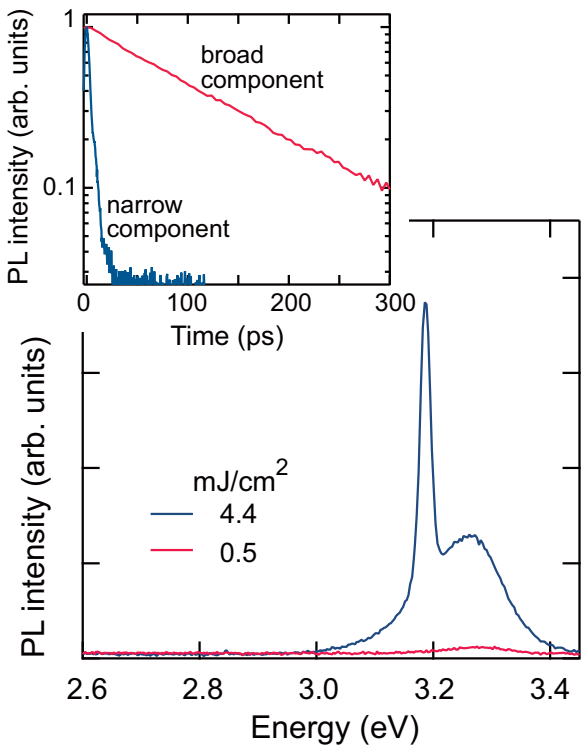

FIG. 3. Room-temperature PL spectra of the micrometer-thick ZnO film obtained under different excitation fluences of femtosecond laser pulses at 350 nm. The inset shows the decay profiles of the broad (red line) and sharp (blue line) emission components.

comes from excitonic stimulated emission with a decay time of <4 ps.

It should be worth mentioning that the peak energy and linewidth of the sharp peak observed in the micrometer-thick film sample are almost constant even when I_{exc} increases far above the threshold ($I_{exc} >\sim 25 I_{exc}^{th}$), as shown in the upper inset in the right panel of Fig. 2(a). Thus, under the present excitation conditions, the excitonic laser emission occurring in the ZnO microcrystals is not concomitant with an EHP emission. This behavior contrasts that of the ZnO nanostructured materials reported previously [3–7,11,17,18] as well as that of the present 85-nm-thick film sample shown in Fig. 2(b). The absence of an EHP implies that the carrier density attained at I_{exc}^{th} is well below $n_M(\sim 10^{18}\,cm^{-3})$ [11,22,30], as will be discussed again in Sec. IV.

C. Temperature-dependent PL characteristics

Figure 4 shows the results of excitation-fluence-dependent PL measurements at 3 K. The PL spectrum obtained under the lowest excitation fluence ($I_{exc} = 0.13\,mJ/cm^2$) shows an emission line at 3.360 eV, which can be attributed to a donor-bound exciton (DBE) emission [31]. At $I_{exc} =\sim 2\,mJ/cm^2$, a new emission peak emerges on the low-energy side of the DBE emission. This peak shows a slight redshift from 3.33 to 3.32 eV with a further increase in I_{exc} [see also Fig. 4(c)]. It should be noted, however, that the half width of the peak remains a constant value of ~20 meV with increasing I_{exc}, indicating that this peak does not result from an EHP emission. The integrated emission intensity of the total emission shows a nonlinear increase with increasing excitation fluence with an excitation threshold of $\sim 2\,mJ/cm^2$ [Fig. 4(b)]. This newly emerged peak in the 3.33−3.23-eV range is attributed to the stimulated emission induced by ex-ex scattering, in which one exciton recombines radiatively while the other is scattered into a higher state ($n = 2,3,...\infty$). The emission maxima of the ex-ex process can be given by [32]

$$\hbar\omega_{max}^{ex-ex}(T) = E_{ex}(T) - E_b\left(1 - \frac{1}{n^2}\right) - \frac{3}{2}k_B T \quad , \qquad (1)$$

where $E_{ex}(T)$ is the free-exciton transition energy at a temperature T, E_b is the binding energy of the exciton (60 meV), and k_B is the Boltzmann constant. According to Eq. (1), the emission maxima at 3 K for $n = 2$ and ∞ are estimated to be 3.332 and 3.316 eV, respectively, on the condition that the $E_{ex}(T) = 3.377$ eV at 3 K [33]. These estimated energies for $n = 2$ and ∞ (3.332 and 3.316 eV) are in reasonable agreement with the upper (3.33 eV) and lower (3.32 eV) limits of the observed peak maxima [see Fig. 4(c)]. This indicates that the micrometer-thick film exhibits the excitonic lasing generated by exciton-exciton scattering at sufficiently low ($T = 3$ K) temperatures.

It is interesting to investigate how the lasing mechanism is influenced by temperature. Hence, we measured the PL spectra of the micrometer-thick film sample in the temperature range from 3 to 300 K under excitation fluence of $I_{exc} = 10.4\,mJ/cm^2$, which is sufficient enough to induce laser emission even at room temperature. As shown in Fig. 5(a), this sample shows a single emission peak with a FWHM of 20–30 meV over the entire temperature range investigated. Note also that the emission peak energy shifts to lower energies especially at temperatures above ~100 K. In Fig. 5(b), we show the temperature dependence of the peak maximum $\hbar\omega_{max}^{obs}(T)$ along with that of the free-exciton transition energy $E_{ex}(T)$ observed for bulk ZnO [33]. One sees from Fig. 5(b) that $\hbar\omega_{max}^{obs}(T)$ shifts faster to lower energies than $E_{ex}(T)$ with increasing temperature. To more clearly show this behavior, we show in Fig. 5(c) the energy difference ΔE between $E_{ex}(T)$ and $\hbar\omega_{max}^{obs}(T)$. For comparison, we also plot the energy difference between $E_{ex}(T)$ and the emission maxima of the ex-ex process $\hbar\omega_{max}^{ex-ex}(T)$ for $n = 2$ and ∞ [see the red broken lines in Fig. 5(c)], which is calculated by modifying the expression of Eq. (1):

$$E_{ex}(T) - \hbar\omega_{max}^{ex-ex}(T) = E_b\left(1 - \frac{1}{n^2}\right) + \frac{3}{2}k_B T. \qquad (2)$$

It is clear from Fig. 5(c) that in the temperature range from 3 to ~150 K, ΔE is located in the energy region between the lines predicted for $n = 2$ and ∞, implying that the ex-ex process is responsible for lasing in this temperature regime. At temperatures above ~150 K, however, ΔE begins to deviate from the energy limit of the ex-ex process for $n = \infty$ and instead shows a zero-intercept linear dependence with temperature. The fitted value of the slope is 5.21×10^{-4} eV/K. Among other excitonic processes, the ex-el process is the only process that is consistent with the observed linear temperature dependence with a zero intercept.

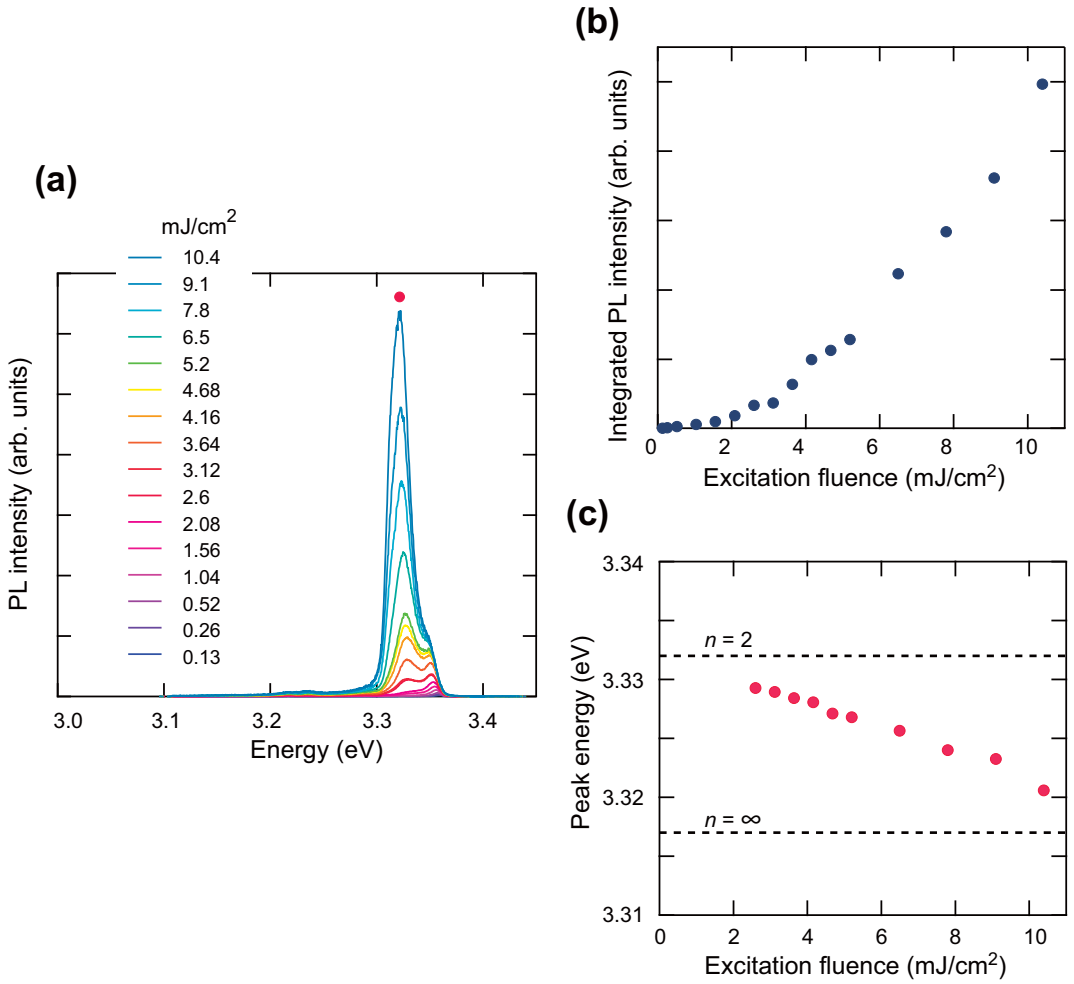

FIG. 4. PL characteristics of the micrometer-thick ZnO film measured at 3 K. (a) Changes in the PL spectra with increasing excitation fluence from 0.13 to 10.4 mJ/cm^2. Excitation fluence dependence of (b) the spectrally integrated PL intensity and (c) the peak energy of the sharp emission component marked by a red filled circle in (a). In (c), the emission maxima of the ex-ex process for $n = 2$ and ∞ at 3 K calculated from Eq. (1) are indicated by dashed lines.

This is because the emission maximum $\hbar\omega_{\max}^{\mathrm{ex-el}}(T)$ of the ex-el process is given by [2,32,34]

$$\hbar\omega_{\max}^{\mathrm{ex-el}}(T) = E_{\mathrm{ex}}(T) - \gamma k_{\mathrm{B}} T, \tag{3}$$

where γ is a constant related to the ratio of exciton effective mass over electron effective mass [34]. The slope of 5.21×10^{-4} eV/K yields the value of $\gamma = 6.1$, which is in reasonable agreement with the predicted value of $\gamma = \sim 7$ [34]. Thus, the observed temperature-dependent energy shift of the emission line elucidates that the excitonic stimulated emission process is changed from ex-ex scattering to ex-el scattering at a temperature of ~150 K. This implies that these two excitonic processes do not coexist with each other; rather, the ex-el process replaces the ex-ex process for $n = \infty$ with increasing temperature above ~150 K. In other words, the threshold lines of carrier concentration for the ex-ex and ex-el lasing processes exhibit a crossover at a temperature of ~150 K. Several transition schemes for the excitonic lasing process with temperature have been predicted previously [22,35–37]; this is an experimental demonstration of the transition or crossover between the ex-ex and ex-el processes on the basis of the temperature-dependent PL measurements that cover a wide temperature region from 3 to 300 K. Note also that except for the peak intensity and peak position, the spectral feature of the lasing bands in Fig. 5(a) remains almost unchanged in the temperature range from 160 to 300 K. This, along with the zero-intercept linear dependence in the 150−300-K range shown in Fig. 5(c), strongly suggests that the ex-el process is able to survive up to room temperature. Thus, it is reasonable to conclude that the room-temperature lasing peak at 3.15–3.17 eV observed in the micrometer-thick film is attributed to the ex-el process. We would also suggest the same assignment is applicable to the room-temperature excitonic process reported previously in high-quality ZnO nanostructured materials since the reported peak energy generally falls within a similar energy range of 3.15−3.20 eV [3–7,22] observed in this work.

IV. DISCUSSION

In Sec. III, we have shown that the present micrometer-thick ZnO film shows purely excitonic lasing at room temperature without showing any symptoms of EHP emission. Since the

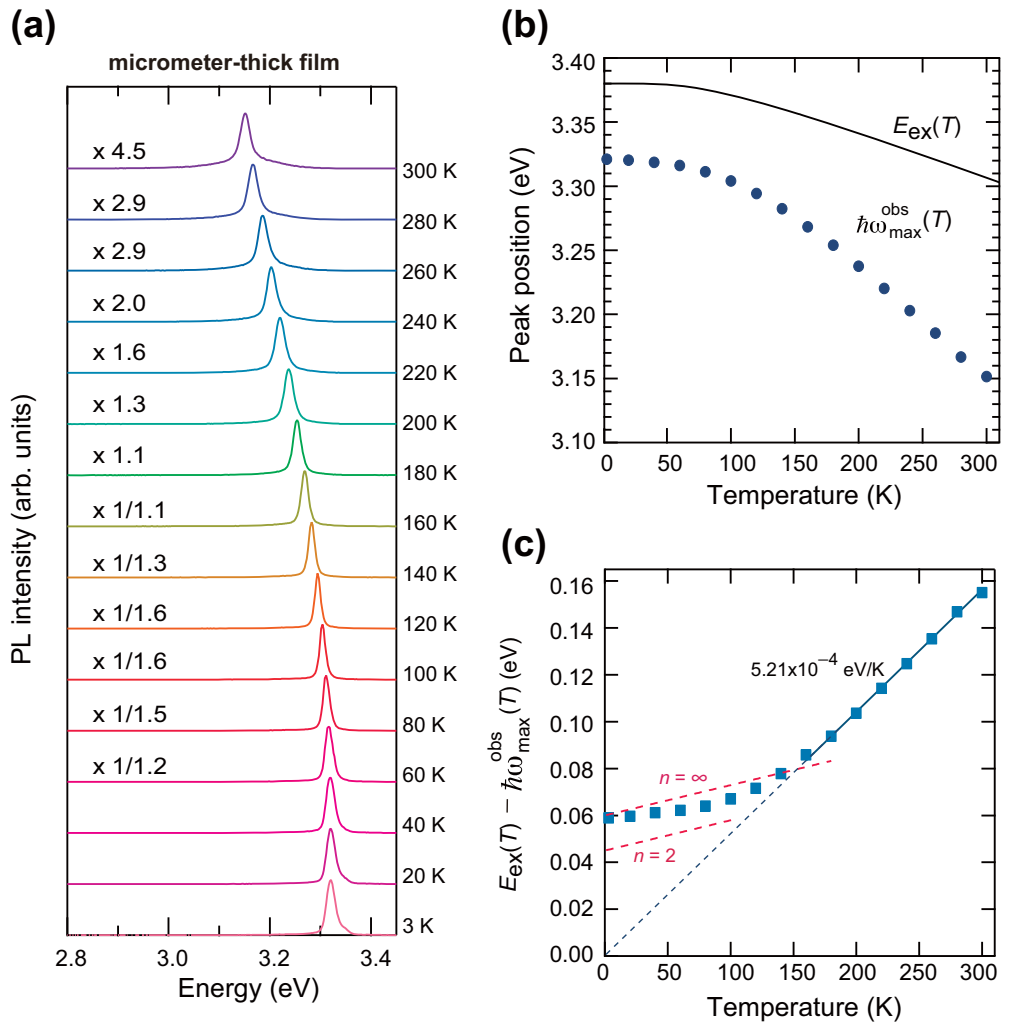

FIG. 5. Temperature dependence of the lasing spectra observed for the micrometer-sized ZnO film. (a) Changes in the lasing spectra with increasing temperature from 3 to 300 K measured under a constant excitation fluence of 10.4 mJ/cm^2. The peak intensities are normalized among all spectra, which are displaced vertically for clarity. (b) The peak energy $\hbar\omega_{max}^{obs}$ as a function of temperature. The free-exciton transition energy E_{ex} reported in Ref. [33] is also shown as a solid line. (c) The energy difference between E_{ex} and $\hbar\omega_{max}^{obs}$ as a function of temperature. The solid line shows a least-squares fit of the data in the temperature region from 160 to 300 K to Eq. (3). The energy differences between $E_{ex}(T)$ and $\hbar\omega_{max}^{ex-ex}(T)$ for $n = 2$ and ∞ calculated from Eq. (2) are also shown as red dashed lines.

exciton-electron collisions are shown to be responsible for the room-temperature excitonic lasing, some of the photogenerated excitons will be thermally ionized. However, the absence of EHP emissions allows us to assume that the total density of photogenerated electron-hole pairs is well below $n_M(\sim 10^{18}$ cm$^{-3})$ [11,22,30] under the present excitation conditions. To confirm this implication, we estimated the density of electron-hole pairs n_p at $I_{th}(\sim 2$ mJ/cm$^2)$ for the micrometer-thick film by assuming that every absorbed photon creates one electron-hole pair as follows [22]:

$$n_p = \frac{P_{exc}\tau}{\hbar\omega_{ext} l}, \tag{4}$$

where P_{exc} and $\hbar\omega_{ext}$ are the excitation power (in W/cm^2) and the photon energy (in J) of the light source, respectively. Under the quasi-stationary excitation regime, which is attained under nanosecond-pulsed excitation, the characteristic time τ can be considered as the decay time of the relevant emission process (spontaneous or stimulated emission). It has been demonstrated that the decay times of the spontaneous and stimulated emissions in ZnO are several hundreds of ps and a few ps, respectively [19,20], in agreement with the present time-resolved measurements shown in Fig. 3. The definition of characteristic length l varies depending on whether the sample size d is larger or smaller than the diffusion length l_D of the excited carriers. That is,

$$l = l_D \quad \text{for} \quad d > l_D, \tag{5}$$

$$l = d \quad \text{for} \quad d < l_D, \tag{6}$$

if the effects of the carrier recombination at surface defects [22] and of the inhibition of carrier diffusion at grain boundaries [38] are neglected. As for wide direct-gap semiconductors with high crystallinity, l_D can be as large as $\sim 3\ \mu$m [32]. This means that the electron-hole pairs created by photoexcitation do not remain confined in a surface layer of a thickness of the reverse

of the one-photon absorption coefficient but rapidly spread out into the volume of the crystal, driven by the gradient of the chemical potential [39]. Thus, it can be assumed that in the present micrometer-thick ZnO sample, l is 3 μm, which is a typical size of the present ZnO microparticles. On the basis of the above considerations, we can estimate the n_p value at I_{th} for the micrometer-thick film sample ($I_{th} = \sim 2\,mJ/cm^2$) on the condition that τ is 4 ps, which is the upper limit of the decay time of the sharp emission component shown in Fig. 3. Thus, for an excitation wavelength of 355 nm with a pulse duration of 10 ns, n_p at $I_{th}(\sim 2\,mJ/cm^2)$ is estimated to be $\sim 5 \times 10^{15}\,cm^{-3}$. This value is almost two orders of magnitude lower than the reported value of $n_M(\sim 10^{18}\,cm^{-3})$ [11,22,30]. Hence, we are almost convinced that the sharp emission peak observed in the micrometer-thick ZnO film is of excitonic origin.

As for the 85-nm-thick film, l should be 85 nm according to Eq. (6), yielding the n_p value of $\sim 2 \times 10^{17} cm^{-3}$ under the same excitation condition of $I_{exc} = \sim 2\,mJ/cm^2$. The resulting n_p value ($\sim 2 \times 10^{17} cm^{-3}$) is just below or close to n_M. This derives from the fact that n_p is inversely proportional to the sample size or the diffusion length of the excited carriers [22]. It is hence reasonable to expect that as compared with micrometer-sized ZnO crystals, ZnO nanocrystals exhibit a more dramatic increase in n_p by a slight change in the excitation intensity, easily reaching the regime of n_M to yield an EHP emission.

The above considerations indicate that the well-crystallized micrometer-sized ZnO crystals are unique in that they exhibit purely excitonic lasing at room temperature under excitation conditions where the density of the photogenerated electron-hole pairs is well below n_M.

V. CONCLUSIONS

We obtained the following two main results from a series of experiments on ZnO with various sizes. First, purely excitonic lasing was observed exclusively from the micrometer-thick film sample over the wide temperature range from 3 K to room temperature; the density of electron-hole pairs at I_{th} is far below the Mott density, showing no sign of the EHP recombination under the excitation conditions employed. Second, we presented the distinct experimental demonstration of the transition of lasing mechanism from the ex-ex scattering to the ex-el scattering at ~150 K. These two processes do not coexist with each other, and the ex-el scattering is the only excitonic process that leads to lasing action in the temperature range from ~150 to 300 K. Since these results are not observed from bulk and nanostructured counterparts, we conclude that the ZnO microcrystals have reasonable advantages in observing and investigating excitonic lasing phenomena in ZnO because of the potential long carrier diffusion length and their inherent low-loss nature.

ACKNOWLEDGMENT

A part of this work was carried out by the Joint Research in the Institute for Solid State Physics, the University of Tokyo.

[1] Ü. Özgür, Ya. I. Alivov, C. Liu, A. Teke, M. A. Reshchikov, S. Dogan, V. Avrutin, S.-J. Cho, and H. Morkoç, J. Appl. Phys. **98**, 041301 (2005).
[2] C. Klingshirn, J. Fallert, H. Zhou, J. Sartor, C. Thiele, F. Maier-Flaig, D. Schneider, and H. Kalt, Phys. Status Solidi B **247**, 1424 (2010).
[3] D. M. Bagnall, Y. F. Chen, Z. Zhu, T. Yao, S. Koyama, M. Y. Shen, and T. Goto, Appl. Phys. Lett. **70**, 2230 (1997).
[4] P. Zu, Z. K. Tang, G. K. L. Wong, M. Kawasaki, A. Ohtomo, H. Koinuma, and Y. Segawa, Solid State Commun. **103**, 459 (1997).
[5] D. M. Bagnall, Y. F. Chen, Z. Zhu, T Yao, M. Y. Shen, and T. Goto, Appl. Phys. Lett. **73**, 1038 (1998).
[6] Ü. Özgür, A. Teke, C. Liu, S. J. Cho, H. Morkoç, and H. O. Everitt. Appl. Phys. Lett. **84**, 3223 (2004).
[7] A.-S. Gadallah, K. Nomenyo, C. Couteau, D. J. Rogers, and G. Lérondel, Appl. Phys. Lett. **102**, 171105 (2013).
[8] M. H. Huang, S. Mao, H. Feick, H. Yan, Y. Wu, H. Kind, E. Weber, R. Russo, and P. Yang, Science **292**, 1897 (2001).
[9] D. Vanmaekelbergh and L. K. van Vugt, Nanoscale **3**, 2783 (2011).
[10] M. Zimmler, F. Capasso, S. Müller, and C. Ronning, Semicond. Sci. Technol. **25**, 024001 (2010).
[11] M. A. M. Versteegh, D. Vanmaekelbergh, and J. I. Dijkhuis, Phys. Rev. Lett. **108**, 157402 (2012).
[12] R. Chen, B. Ling, X. W. Sun, and H. D. Sun, Adv. Mater. **23**, 2199 (2011).
[13] D. Yu, Y. Chen, B. L. Chen, M. Z. Zhao, and S. Ren, Appl. Phys. Lett. **91**, 091116 (2007).
[14] D. J. Gargas, M. C. Moore, A. Ni, S.-W. Chang, Z. Zhang, S.-L. Chuang, and P. Yang, ACS Nano **4**, 3270 (2010).
[15] H. Cao, Y. G. Zhao, S. T. Ho, E. W. Seelig, Q. H. Wang, and R. P. H. Chang, Phys. Rev. Lett. **82**, 2278 (1999).
[16] J. Fallert, R. J. B. Dietz, J. Sartor, D. Schneider, C. Klingshirn, and H. Kalt, Nat. Photon. **3**, 279 (2009).
[17] T. Nakamura, K. Firdaus, and S. Adachi, Phys. Rev. B **86**, 205103 (2012).
[18] K. Suzuki, M. Inoguchi, K. Fujita, S. Murai, K. Tanaka, N. Tanaka, A. Ando and H. Takagi, J. Appl. Phys. **107**, 124311 (2010).
[19] W. M. Kwok, A. B. Djurišić, Y. H. Leung, W. K. Chan, and D. L. Phillips, Appl. Phys. Lett. **87**, 093108 (2005).
[20] A. B. Djurišić, W. M. Kwok, Y. H. Leung, D. L. Phillips, and W. K. Chan, J. Phys. Chem. B **109**, 19228 (2005).
[21] D. M. Bagnall, in *Zinc Oxide Materials for Electronic and Optoelectronic Devices and Applications*, edited by C. W. Litton, D. C. Reynolds, and T. C. Collins (Wiley, Chichester, 2011). pp. 265–284.
[22] C. Klingshirn, R. Hauschild, J. Fallert, and H. Kalt, Phys. Rev. B **75**, 115203 (2007).
[23] C. Klingshirn, J. Fallert, O. Gogolin, M. Wissinger, R. Hauschild, M. Hauser, H. Kalt, and H. Zhou, J. Lumin. **128**, 792 (2008).
[24] T. Okada, K. Kawashima, and M. Ueda, Appl. Phys. A **81**, 907 (2005).
[25] K. Okazaki, T. Shimogaki, K. Fusazaki, M. Higashihata, and D. Nakamura, Appl. Phys. Lett. **101**, 211105 (2012).

[26] T. Nakamura, S. Sonoda, T. Yamamoto, and S. Adachi, Opt. Lett. **40**, 2662 (2015).
[27] H. Cao, in *Progress in Optics*, edited by E. Wolf (Elsevier, Amsterdam, 2003) Vol. 45, pp. 317–370.
[28] G. van Soest and A. Lagendijk, Phys. Rev. E **65**, 047601 (2002).
[29] E. M. Kaidashev, M. Lorenz, H. von Wenckstern, A. Rahm, H.-C. Semmelhack, K.-H. Han, G. Benndorf, C. Bundesmann, H. Hochmuth, and M. Grundmann, Appl. Phys. Lett. **82**, 3901 (2003).
[30] A. Schleife, C. Rödl, F. Fuchs, K. Hannewald, and F. Bechstedt, Phys. Rev. Lett. **107**, 236405 (2011).
[31] M. R. Wagner, G. Callsen, J. S. Reparaz, J.-H. Schulze, R. Kirste, M. Cobet, I. A. Ostapenko, S. Rodt, C. Nenstiel, M. Kaiser, A. Hoffmann, A. V. Rodina, M. R. Phillips, S. Lautenschläger, S. Eisermann, and B. K. Meyer, Phys. Rev. B **84**, 035313 (2011).
[32] C. Klingshirn, *Semiconductor Optics*, 3rd ed. (Springer, Berlin, 2007).
[33] L. Wang and N. C. Giles, J. Appl. Phys. **94**, 973 (2003).
[34] C. Klingshirn, Phys. Status Solidi B **71**, 547 (1975).
[35] B. Hönerlage, C. Klingshirn, and J. B. Grun, Phys. Status Solidi B **78**, 599 (1976).
[36] H. Haug and S. Koch, Phys. Status Solidi B **82**, 531 (1977).
[37] S. W. Koch, H. Haug, G. Schmieder, W. Bohnert, and C. Klingshirn, Phys. Status Solidi B **89**, 431 (1978).
[38] G. Tobin, E. McGlynn, M. O. Henry, J.-P. Mosnier, E. de Posada, and J. G. Lunney, Appl. Phys. Lett. **88**, 071919 (2006).
[39] C. Klingshirn and H. Haug, Phys. Rep. **70**, 315 (1981).